Wnt and CDK-1 regulate cortical release of WRM-1/beta-catenin to control cell division orientation in early Caenorhabditis elegans embryos

Wnt and CDK-1 regulate cortical release of WRM-1/β-catenin to control cell division orientation in early *Caenorhabditis elegans* embryos

Soyoung Kim[a,1], Takao Ishidate[a,b,1], Rita Sharma[a,b], Martha C. Soto[c], Darryl Conte, Jr.[a], Craig C. Mello[a,b,2], and Masaki Shirayama[a,b,2]

[a]Program in Molecular Medicine and [b]Howard Hughes Medical Institute, University of Massachusetts Medical School, Worcester, MA 01605; and [c]Department of Pathology, University of Medicine and Dentistry of New Jersey—Robert Wood Johnson Medical School, Piscataway, NJ 08854

Contributed by Craig C. Mello, January 22, 2013 (sent for review December 9, 2012)

In early *Caenorhabditis elegans* embryos, the Wingless/int (Wnt)- and Src-signaling pathways function in parallel to induce both the division orientation of the endomesoderm (EMS) blastomere and the endoderm fate of the posterior EMS daughter cell, called E. Here, we show that, in addition to its role in endoderm specification, the β-catenin–related protein Worm armadillo 1 (WRM-1) also plays a role in controlling EMS division orientation. WRM-1 localizes to the cortex of cells in both embryos and larvae and is released from the cortex in a Wnt-responsive manner. We show that WRM-1 cortical release is disrupted in a hypomorphic *cyclin-dependent protein kinase 1* (*cdk-1*) mutant and that WRM-1 lacking potential CDK-1 phosphoacceptor sites is retained at the cortex. In both cases, cortical WRM-1 interferes with EMS spindle rotation without affecting endoderm specification. Finally, we show that removal of WRM-1 from the cortex can restore WT division orientation, even when both Wnt- and Src-signaling pathways are compromised. Our findings are consistent with a model in which Wnt signaling and CDK-1 modify WRM-1 in a temporal and spatial manner to unmask an intrinsic polarity cue required for proper orientation of the EMS cell division axis.

cell polarity | embryogenesis | asymmetric cell division | Src signaling

The control of cell division orientation is of fundamental importance in both development and tissue homeostasis (1–4). In nonpolarized cells, the centrosome duplication and migration cycle result in nascent asters positioned at 90° relative to the previous division axis. Thus, in the absence of intrinsic asymmetries or signals from neighboring cells, the default cleavage program is to divide orthogonally at each subsequent division. Studies on the polarized early cell divisions of the nematode *Caenorhabditis elegans* have led to fundamental insights into conserved mechanisms underlying the control of cell division orientation. In *C. elegans*, anterior–posterior (a-p) polarity is established soon after fertilization in response to a symmetry-breaking cue provided by the sperm (5). As a result, conserved cytoplasmic partitioning (PAR) proteins adopt asymmetric cortical associations along the a-p axis. PAR-2 localizes at the posterior cortex and restricts a PAR-3/PAR-6 complex to the anterior cortex (6). These factors, in turn, create regional differences in cortical properties and microtubule dynamics that result in an asymmetric distribution of cytoplasmic contents and an initial cleavage furrow that is displaced to the posterior pole of the one-cell embryo (7). In both blastomeres of the two-cell embryo, AB and P1, centrosomes duplicate, and the daughter centrosomes migrate to opposite sides of the nucleus, 90° from the a-p axis. In the AB blastomere, the spindle forms along this new axis that is perpendicular to the a-p axis. In P1, however, the centrosome–nuclear complex rotates 90°, and the spindle forms along the a-p axis in a manner dependent on the *par* gene products. In *par-2* mutants, the P1 centrosome–nuclear complex fails to rotate, and the spindle forms perpendicular to the a-p axis. In *par-3* mutants, the spindle rotates in both AB and P1 blastomeres, and both cells divide along the a-p axis. Interestingly, the AB and P1 spindles also rotate in *par-2*; *par-3* double mutants, just as in *par-3* mutants, suggesting a possibility that neither gene is required for spindle rotation (8). Although the phenotype still needs to be confirmed with null alleles, the current model to explain this genetic interaction is that PAR-3 prevents rotation of the spindle by masking intrinsic cortical cue(s) and that PAR-2 restricts PAR-3 activity to the AB cell (8). The epistasis tests also suggest that the early blastomeres harbor intrinsic polarity cues that can capture astral complexes and induce rotation of the spindle apparatus onto the a-p axis.

The endomesoderm (EMS) blastomere in the four-cell embryo is the first to be polarized through cell–cell communication. Although EMS does not exhibit an a-p asymmetry of PAR proteins (9, 10), it nevertheless rotates its spindle complex onto the a-p axis and divides to produce an anterior mesodermal precursor, MS, and a posterior cell, E, that produces exclusively endoderm. Classical embryologic studies have shown that the EMS blastomere in a partial embryo, from which P2 has been removed, divides symmetrically without orienting its division axis and produces two daughters that divide and differentiate like WT MS cells. If EMS is placed in contact with an isolated P2 blastomere, EMS becomes polarized, establishes a longitudinal division axis, and divides to produce an E daughter adjacent to P2 and a distal MS daughter (11–14). This cell–cell interaction (hereafter referred to as P2/EMS signaling) depends on parallel inputs from the Wingless/int (Wnt)- and Src-related signaling pathways (15–18). Mutation or RNAi of either Wnt- or Src-signaling components

Significance

Cellular asymmetry, or polarity, is essential for development and tissue homeostasis. In *Caenorhabditis elegans*, the conserved Wnt signal transduction pathway orients the cell division axis and polarizes the EMS blastomere to promote endoderm fate. This work provides a mechanism for how the Wnt/β-catenin pathway integrates spatial and temporal cues important for the cell division axis. We show that CDK-1 phosphorylates and promotes the release of cortical β-catenin, which brings Wnt signaling under cell cycle control and facilitates spindle rotation. Cell cycle control of developmental decisions may be particularly important in embryos or tissues that undergo rapid cell divisions and patterning.

Author contributions: S.K., T.I., M.C.S., C.C.M., and M.S. designed research; S.K., T.I., R.S., and M.S. performed research; S.K., T.I., and M.S. contributed new reagents/analytic tools; S.K., T.I., C.C.M., and M.S. analyzed data; and S.K., T.I., D.C., C.C.M., and M.S. wrote the paper.

The authors declare no conflict of interest.

Freely available online through the PNAS open access option.

[1]S.K. and T.I. contributed equally to this work.

[2]To whom correspondence may be addressed. E-mail: craig.mello@umassmed.edu or masaki.shirayama@umassmed.edu.

This article contains supporting information online at www.pnas.org/lookup/suppl/doi:10.1073/pnas.1300769110/-/DCSupplemental.

results in, at most, partial defects in EMS division orientation and endoderm induction. Fully penetrant defects in EMS polarity are observed only if both pathways are compromised simultaneously.

WRM-1 (Worm armadillo 1), a homolog of β-catenin, plays a central role in cell fate specification downstream of P2/EMS signaling (16), but it has not been implicated in the control of EMS division orientation (19). In embryos and larvae, WRM-1 localizes uniformly at the cell cortex and in nuclei. In Wnt-responsive cells, however, WRM-1 is released from the cortex and accumulates to slightly higher levels in the nucleus of the posterior daughter cell, which seems to be critical for cell fate determination (20–22). RNAi of *wrm-1* has no effect on EMS division orientation but results in a fully penetrant loss of endoderm, suggesting that the Wnt and Src signals converge on WRM-1 to specify the endoderm fate (19).

Here, we show that cortical release of WRM-1 permits proper EMS division orientation. In *cyclin-dependent protein kinase 1* (*cdk-1*) mutant embryos or embryos expressing a WRM-1 protein lacking potential CDK-1 phosphoacceptor sites, WRM-1 is retained at the cortex and although capable of endoderm specification, interferes with EMS division orientation when Src signaling is defective. Finally, we show that removal of WRM-1 from the cortex restores WT division orientation, even when both Wnt and Src signaling are compromised. Taken together, these findings are consistent with a model whereby WRM-1, in a manner analogous to the PAR-3/PAR-6 complex, masks a cortical site required for EMS division axis rotation until temporal cues from CDK-1 and spatial cues from Wnt induce its cortical release.

Results

WRM-1 Is Released from the Cortex of EMS During Mitotic Prophase. We previously found that WT GFP::WRM-1 was localized to all nuclei and all cell–cell contacts throughout early embryogenesis (21) (Fig. 1 and Figs. S1 and S2). However, we observed a dramatic loss of GFP::WRM-1 from the posterior cortex of EMS adjacent to the signaling cell P2 at the six-cell stage (21) (Fig. 1 *A* and *B*). To examine when cortical release of GFP::WRM-1 takes

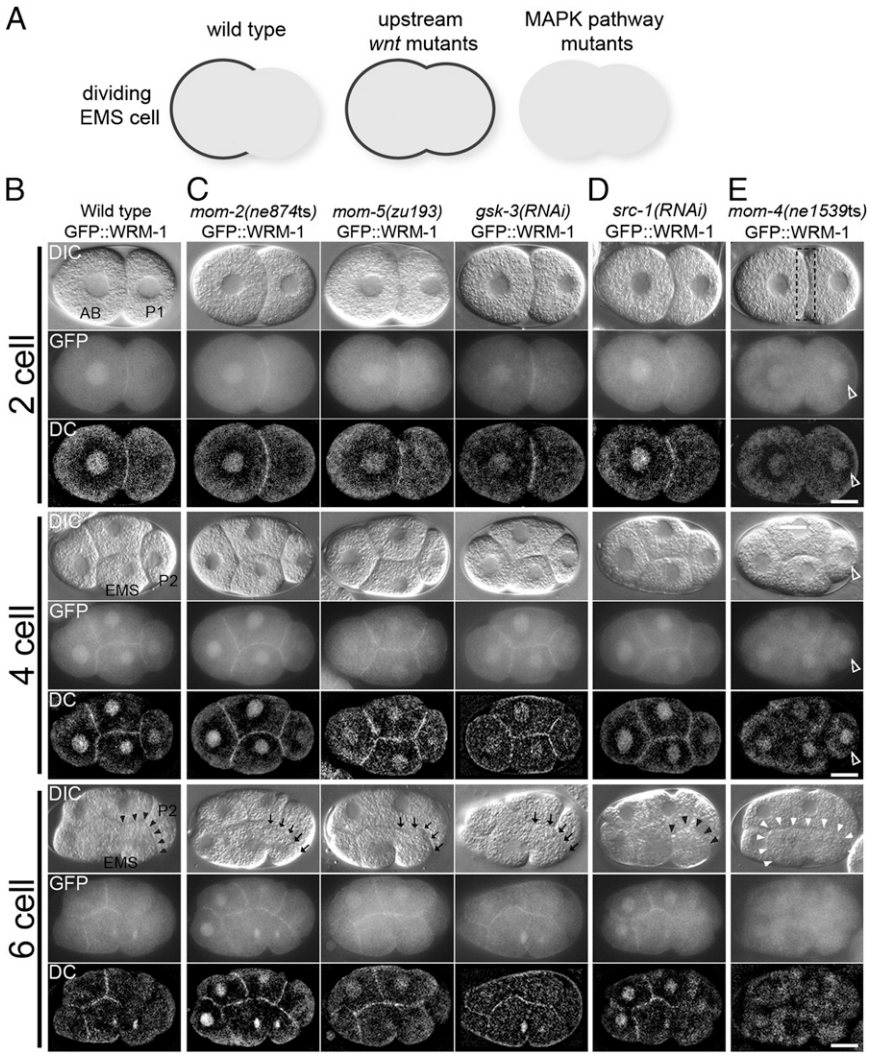

Fig. 1. WRM-1 cortical localization is regulated by Wnt and MAPK-like pathways in early embryos. (*A*) A schematic representation of GFP::WRM-1 localization in dividing EMS cell in indicated genetic backgrounds. Cortical GFP signal is depicted by a thick black line. (*B–E*) Nomarsky (DIC), fluorescence (GFP), and deconvoluted fluorescence (DC) micrographs of two-, four-, and six-cell stages (or late four-cell stage) embryos expressing GFP::WRM-1 in (*B*) WT background, (*C*) upstream Wnt pathway mutants, (*D*) Src, and (*E*) MAPK-like pathway mutants indicated. Black arrowheads indicate absence of cortical WRM-1, and black arrows indicate retention of WRM-1 on the posterior EMS cortex. In *E*, white arrowheads indicate entire EMS cortex without cortical WRM-1 localization. Dotted box in two-cell stage indicates the absence of cortical WRM-1 at AB and P1 boundary, whereas empty arrowheads indicate ectopic accumulation of nuclear WRM-1 in P1 and P2 cells. Anterior is to the left, and dorsal is up. AB, P1, P2, and EMS cells are indicated in the WT DIC panels. (Scale bar: 10 μm.)

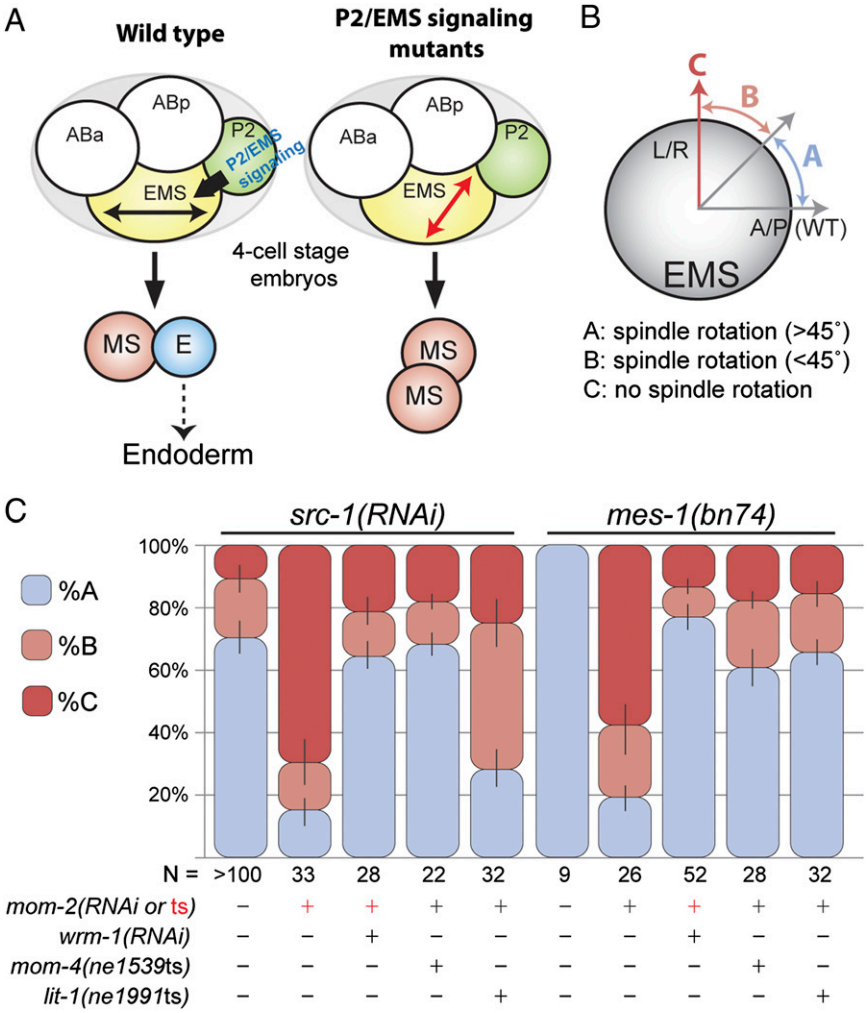

Fig. 2. *wrm-1* suppresses the EMS spindle orientation defect of *wnt; src* double mutants. (*A*) Model depicting the rotation of EMS mitotic spindle to a-p orientation (black double-headed arrow) from the default l-r orientation (red double-headed arrow) in response to P2/EMS signal. In P2/EMS signaling mutants, EMS mitotic spindle fails to rotate, and induction of E cell fate does not occur. (*B*) Schematic representation of the EMS mitotic spindle orientation categories (A, B, and C) analyzed in *C*. A/P denotes a-p axis. L/R denotes l-r axis. Details on the scoring method are in *Materials and Methods*. (*C*) Stacked bar graphs show the percentage of EMS cells exhibiting each mitotic spindle orientation category depicted in *B* in various genetic backgrounds shown. RNAi treatments or presence of mutant alleles are specified by +. For *mom-2*, + in red indicates the existence of *mom-2(ne834*ts*)* allele, and *mom-2(RNAi)* treatment is shown with black +. In double *RNAi* knockdown experiments, *src-1* knockdown was always confirmed first by checking the phenotype of *src-1*(*RNAi*) dead embryos before the animals were subjected to *wrm-1* or *mom-2* (*RNAi*). N, number of embryos scored.

place during the cell cycle, we compared the timing of loss of GFP::WRM-1 with the timing of chromosome condensation by using the strain expressing an mCherry::Histone 2B reporter. We found that cortical release of WRM-1 takes place during prophase while the chromosomes are condensing but before the spindle initiates its rotation onto the a-p axis of the cell ($n = 20$). The area of cortical depletion seemed to initiate at the P2/EMS junction and extend gradually to the cleavage furrow of EMS (Fig. 1*B*). A similar cortical depletion was also observed in the regions of contact between P2 and ABp descendants; however, the biological relevance of WRM-1 release in ABp descendants is currently unknown. After the division of EMS, the posterior E blastomere inherited the cortical region depleted of WRM-1 (Fig. S2*A*) and developed a relatively high nuclear accumulation of GFP::WRM-1 compared with its anterior sister MS (21) (Fig. S2 *A* and *G*).

Cortical Localization of WRM-1 in the P2/EMS Signaling Mutants. We next explored how WRM-1 localization was affected by previously described P2/EMS signaling components (Fig. 1 and Figs. S1 and S2). Our previous preliminary studies with a faint GFP::WRM-1 signal suggested that the Frizzled homolog More mesoderm 5 (MOM-5) is required for the initial cortical association of WRM-1 in all embryonic cells (21). However, our current analysis with improved GFP strains unequivocally revealed that loss of function of any upstream Wnt signaling-related factors, including Frizzled (MOM-5), Wnt (MOM-2), Dishevelled (DSH-1, DSH-2, and MIG-5), and Glycogen synthase kinase 3β (GSK-3), results in identical phenotypes with respect to WRM-1 localization. In each mutant, the cortically localized WRM-1 remains uniform throughout the EMS division (Fig. 1*C* and Fig. S1 *A* and *F*). As previously reported (21), the asymmetric nuclear accumulation of WRM-1 in the E blastomere was also abolished in each of the Wnt-signaling defective strains (Fig. S2 *A* and *G*).

The Wnt- and Src-signaling pathways act together to specify EMS division orientation and endoderm fate. We, therefore, asked whether the Src-signaling components, Maternal effect sterile 1 (MES-1) and SRC-1, are required for the cortical localization and release of WRM-1. We found that WRM-1 exhibited WT cortical localization and release in 100% of *mes-1* (*bn74*) null mutants at 25 °C, which lack the entire *mes-1* coding

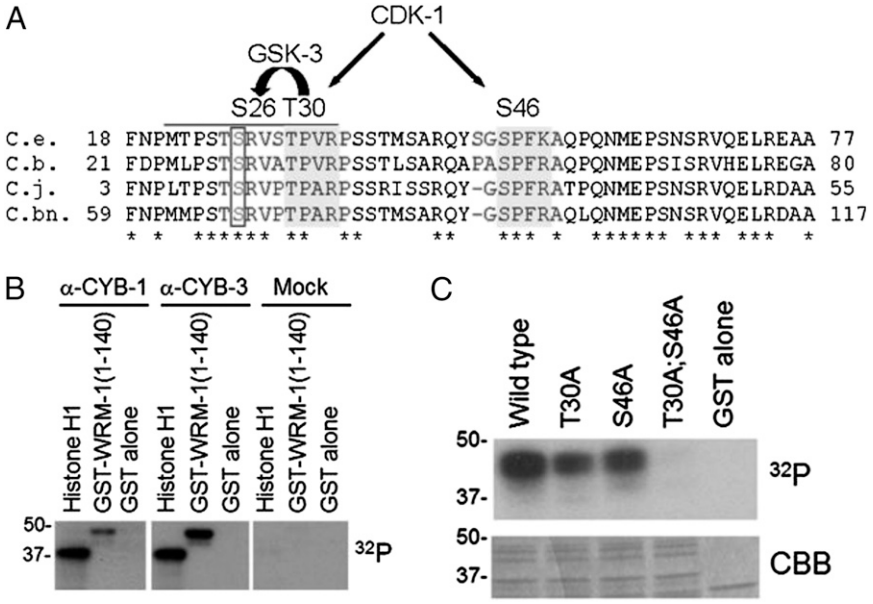

Fig. 3. WRM-1 is phosphorylated by CDK-1 in vitro. (*A*) Amino acid alignments of an N-terminal region of WRM-1 from *C. elegans* (C.e.) and related nematodes *C. briggsae* (C.b.), *C. japonica* (C.j.), and *C. brennei* (C.bn.). Conserved CDK-1 consensus sites are highlighted in dark gray. Conserved GSK-3 site that is coupled to the CDK-1 site is boxed. Phosphoacceptor residues are indicated above the alignment. (*B*) In vitro phosphorylation of WRM-1(1-140) by CYB-1 (α-CYB-1), CYB-3 (α-CYB-3), or control (mock) immune complexes. Histone H1 is provided as a positive control substrate, and GST alone is provided as a negative control substrate. (*C*) In vitro phosphorylation of WRM-1(1-140) substrates by human recombinant CDC2/Cyclin B kinase. Mutations in CDK-1 phosphoacceptor residues are indicated. CBB, Coomassie Brilliant Blue.

region (23), and 72% of *src-1*(*RNAi*) embryos (Fig. 1*D* and Fig. S1 *B* and *F*). The knockdown of *src-1* by RNAi seemed to be complete, because 100% of *src-1*(*RNAi*) embryos ($n > 100$) arrested with a complete lack of body morphogenesis, which is characteristic of *src-1* null mutant embryos (15). Furthermore, early *src-1*(*RNAi*) embryos exhibited a lack of cortical staining with the phosphotyrosine-specific monoclonal antibody pY99, indicative of strongly depleted SRC-1 activity (15). Asymmetric nuclear accumulation of WRM-1 in the E blastomere was also dependent on SRC-1 but not MES-1 (Fig. S2 *B* and *G*). These differences between the *mes-1* and *src-1* phenotypes may reflect the fact that a basal level of SRC-1 activity persists at all cell contact sites, even in the absence of the upstream activator MES-1 (15). Taken together, these findings indicate that Src signaling is only partially required and less critical than Wnt signaling to regulate WRM-1 cortical release.

The MAPK-related signaling components MOM-4 (MAPKKK) and LIT-1 (MAPK-like) also contribute to EMS specification (24–26). However, in striking contrast to the Wnt or Src pathways, we never observed GFP::WRM-1 at the cortex of any cells of *mom-4* or *lit-1* mutant embryos (Fig. 1*E* and Figs. S1 *C* and *F* and S2*C*), suggesting that the activities of MOM-4 and LIT-1 are required in all cells to induce cortical localization of WRM-1.

Cortical WRM-1 Interferes with Spindle Rotation in EMS. Although previous studies had shown that WRM-1 is not required for EMS spindle rotation, we wondered if cortical retention of WRM-1 might explain why the EMS spindle fails to rotate in P2/EMS signaling mutants. To test this idea, we examined spindle orientation in *mom-4* and *lit-1* temperature-sensitive mutants, where WRM-1 is expressed but fails to localize to the cortex. We found that the EMS spindle orientation defects in *mom-2*; *src-1* or *mom-2*; *mes-1* double mutants are rescued by mutations in *mom-4* or *lit-1* (Fig. 2 and Table S1). As a second and more direct test of the idea that WRM-1 can interfere with EMS spindle rotation, we asked if removing WRM-1 by RNAi could restore proper EMS a-p division orientation in the Wnt and Src pathway double mutants. Strikingly, in all contexts analyzed, RNAi of *wrm-1* suppressed the spindle orientation defects in EMS to levels observed in *src-1*(*RNAi*) embryos (Fig. 2 and Table S1). These results suggest that an a-p division orientation represents a ground state for the EMS cell and that cortical retention of WRM-1 interferes with spindle rotation.

Previous studies using isolated blastomeres showed that both Wnt and Src signaling actively direct the orientation of the EMS division axis (5, 11–15). Our current findings suggest that Wnt signaling might also permit proper division orientation by removing an otherwise inhibitory factor, WRM-1, from the posterior cortex of EMS. To test whether Wnt signaling orients the EMS division axis solely by regulating WRM-1 cortical release, we isolated and reconstituted P2 and EMS from *mom-2*(*ne141*); *wrm-1*(*RNAi*) double-mutant embryos. We found that EMS blastomeres isolated from *mom-2; wrm-1* mutants failed to orient the EMS division axis when placed in contact with P2 [14% (n = 7) in *mom-2*; *wrm-1*, 0% (n = 4) in *mom-2*, and 100% (n = 5) in WT], indicating that removing WRM-1 suppresses *mom-2* mutants in orienting division axis only in intact embryos but not isolated EMS. This finding supports the previous conclusion that Wnt signaling actively controls division orientation beyond its role in regulating WRM-1 cortical release (5, 11–15). Because removing WRM-1 can rescue EMS a-p division orientation in intact *mom-2* embryos, these findings suggest that the process of isolating blastomeres and reconstituting cell contacts destroys an intrinsic cue or perhaps, simply removes a point of reference necessary for detecting an intrinsic a-p polarity cue normally present in EMS. Alternatively, it is possible that the relatively round cell shape of isolated blastomeres disrupts a geometry-driven nuclear rotation that may occur in the unaltered *wrm-1* embryo, similar to the geometry-dependent division described in *par-3* mutants (27). Consistent with this model, a recent paper has shown that Wnt signaling and geometric cues redundantly control the seam cell division axis in *C. elegans* (28).

WRM-1 Is a Target of CDK-1 Kinase. The timing of WRM-1 cortical release at prophase of the EMS cell division suggested that the cell cycle machinery regulates WRM-1. To explore the possibility

of direct regulation of WRM-1 by CDK-1, we used the program Scansite (29) to search for potential CDK-1 sites in the WRM-1 protein. We identified two potential CDK-1 sites in the N-terminal region of WRM-1 that are conserved among related nematode species (Fig. 3*A*). We found that a 140-aa N-terminal peptide containing both CDK-1 sites was robustly phosphorylated in vitro by CDK-1/CYB-1 (Cyclin B1) and CDK-1/CYB-3 (Cyclin B3) complexes that were immunoprecipitated from worm embryo extracts (Fig. 3*B*) and a commercially available vertebrate CDC2 (Cell division control 2)/Cyclin B complex (Fig. 3*C*). A mutation in either of the CDK-1 sites (T30A or S46A) reduced the phosphorylation by CDC2/Cyclin B, whereas the double mutation completely abolished phosphorylation (Fig. 3*C*), indicating that T30 and S46 are both phosphorylated in vitro.

We noticed that T30 is situated such that phosphorylation by CDK-1 could prime WRM-1 for subsequent phosphorylation by GSK-3 at serine 26 (S26) (Fig. 3*A*). Indeed, WRM-1 peptides were robustly phosphorylated by recombinant GSK3β in a manner dependent on both preincubation with CDC2/Cyclin B and the presence of the intact CDK-1 site (T30) (Fig. S3). However, mutation of S26 to alanine had only a minor affect on WRM-1 cortical localization and resulted in no detectable phenotype (Figs. S1 *E* and *F* and S2*F*). GSK-3 phosphorylation of this residue may be relevant at some other developmental stage but was not investigated further in this study.

Previous work has shown that WRM-1 binds to the MAPK-like protein, LIT-1, to form an active kinase complex that phosphorylates WRM-1 and the transcription factor POP-1 (Posterior pharynx defect 1) (25). To examine the effect of CDK-1 phosphorylation on WRM-1–LIT-1 interaction, we expressed WRM-1 with WT or mutant CDK-1 phosphoacceptor sites together with LIT-1 in mammalian cells and immunoprecipitated WRM-1/LIT-1 complexes. Recombinant WRM-1 proteins with mutations in the potential CDK-1 phosphorylation sites formed stable and active WRM-1/LIT-1 kinase complexes in vitro (Fig. S4). Our in vitro biochemical assays suggest that phosphorylation of WRM-1 by CDK-1 and LIT-1 is independent of each other and that CDK-1 phosphorylation does not affect the ability of WRM-1 to bind to and activate the LIT-1 kinase.

WRM-1 Localization Is Regulated by CDK-1 Kinase. To examine the significance of WRM-1 phosphorylation by CDK-1 in vivo, we generated a series of *wrm-1* transgene constructs bearing WT or mutant CDK-1 phosphoacceptor sites (T30A; S46A). These constructs were generated both with and without *flag* and *gfp* tags and integrated into the genome by microparticle bombardment (30) or homologous recombination into a defined chromosomal location (31) (*Materials and Methods*). Immunoblotting with FLAG-specific antibodies confirmed that the WT and phosphoacceptor mutant (T30A; S46A) WRM-1 proteins were expressed at identical levels. Surprisingly, both *wrm-1*(WT) and *wrm-1*$_{T30A\ S46A}$ single-copy transgenes fully and equally rescue all aspects of a *wrm-1* null mutation, *wrm-1*(*tm514*), which exhibits zygotic embryonic lethal and sterile phenotypes.

Despite its ability to rescue the *wrm-1* mutant to viability, the GFP::WRM-1$_{T30A\ S46A}$ fusion protein failed to dissociate from the posterior cortex during the EMS cell cycle (Fig. 4 and Fig. S1*F*) and accumulated to equal levels in the nuclei of MS and E ($n > 20$) (Fig. S2*F*). RNAi of *cdk-1* results in embryos that arrest at the one-cell stage (32). Therefore, to examine the regulation of WRM-1 localization in *cdk-1* mutants, we took advantage of a conditional allele of *cdk-1*(*ne2257*ts), which had previously been implicated in EMS specification (33). At the restrictive temperature of 25 °C, *cdk-1*(*ne2257*ts) embryos undergo WT cell di-

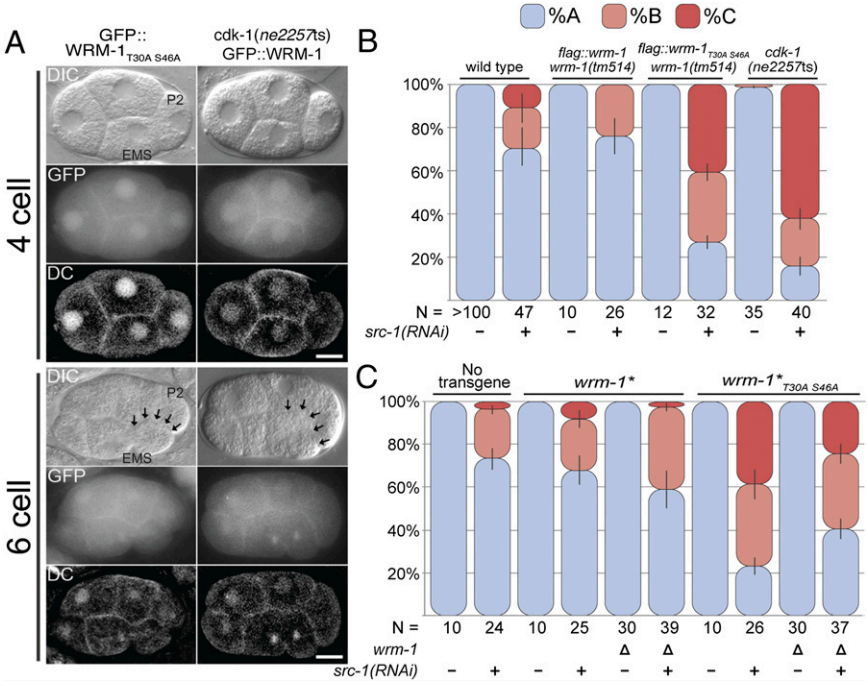

Fig. 4. CDK-1 promotes cortical release of WRM-1 to regulate spindle orientation. (*A*) Nomarsky (DIC), fluorescence (GFP), and deconvoluted fluorescence (DC) micrographs of four- and six-cell stages (or late four-cell stage) embryos expressing GFP::WRM-1$_{T30AS46A}$ (*Left*) or GFP::WRM-1 (*Right*) in *cdk-1(ne2257*ts*)* background at 20 °C. Black arrows indicate retention of WRM-1 on the posterior EMS cortex. Anterior is to the left, and dorsal is up. P2 and EMS cells are indicated in the WT DIC panels. (Scale bar: 10 μm.) (*B*) Stacked bar graphs as in Fig. 2. EMS spindle rotation defect is enhanced in the transgenic line harboring *flag::wrm-1*$_{T30AS46A}$ but not *flag::wrm-1*transgene as well as in *cdk-1(ne2257*ts*)* mutant grown at 20 °C when treated with *src-1*(*RNAi*). *wrm-1*(*tm514*) is a deletion allele of *wrm-1*. (*C*) EMS cell polarity was analyzed using strains expressing *wrm-1* transgenes without an epitope tag (*wrm-1** and *wrm-1**$_{T30AS46A}$) in *wrm-1* deletion (Δ) and WT background. N represents the number of embryos scored.

vision cycles but exhibit defects in endoderm specification and a left–right (l-r) rather than a-p orientation of the EMS cell division (33). Under these conditions, *cdk-1*(*ne2257*ts) mutants exhibit pleiotropic defects in the specification of the P2 cell fate that correlated with the mislocalization of the cell fate determinant OMA-1 (Oocyte maturation defective 1) (33). At the permissive temperature of 20 °C, however, we found that *cdk-1* (*ne2257*ts) embryos are viable and exhibit WT regulation of the OMA-1 protein (Fig. S5). Interestingly, we found that these viable *cdk-1*(*ne2257*ts) embryos retain WRM-1 protein at the cortex throughout the EMS cell cycle (Fig. 4*A* and Fig. S1*F*) and exhibit symmetric accumulation of WRM-1 protein in the nuclei of E and MS (Fig. S2 *E* and *G*). Thus, the CDK-1 phosphoacceptor site mutations (T30A; S46A) in WRM-1 and the *cdk-1*(*ne2257*ts) mutant cultured at 20 °C resulted in identical defects in the cortical and nuclear localization of WRM-1 protein. These in vivo genetic data, along with the biochemical data showing CDK-1–dependent phosphorylation of WRM-1 peptides in vitro, support a potential direct regulation of WRM-1 by CDK-1 phosphorylation. These results also suggest that the cortical retention and symmetric nuclear localization of WRM-1 can be tolerated for both gut induction and viability.

CDK-1 Functions with Wnt Signaling to Control Spindle Orientation. As mentioned above, the orientation of the EMS cell division and endoderm induction are specified through parallel inputs from the Src- and Wnt-signaling pathways. We, therefore, asked if the *wrm-1*$_{T30A\ S46A}$ or *cdk-1*(*ne2257*ts) strains synergize with Wnt- or Src-signaling mutants. Consistent with a role for CDK-1 in the Wnt-dependent regulation of WRM-1, we observed synergistic defects in the orientation of the EMS cell division combined with Src- but not Wnt-pathway components (Figs. 4 *B* and *C* and 5 and Tables S1 and S2). Synergy was also observed with each of the independently generated *wrm-1*$_{T30A\ S46A}$ transgenic lines, including the *flag*-tagged (Fig. 4*B*) and untagged lines (Fig. 4*C*). Interestingly, synergy still occurred and was slightly enhanced when the *wrm-1*$_{T30A\ S46A}$ transgene was expressed in animals that contain WT *wrm-1* at the endogenous locus (Fig. 4*C*). This result suggests that WT WRM-1 is not completely excluded from the cortex and that the effect of the WRM-1$_{T30A\ S46A}$ protein on spindle orientation is exacerbated by the presence of WT WRM-1. Finally, consistent with the idea that inappropriate WRM-1 activity underlies these effects, we found that *wrm-1*(*RNAi*) or mutations in *mom-4* or *lit-1* suppress the EMS division orientation defects of *wrm-1*$_{T30A\ S46A}$; *src-1*(*RNAi*) and *cdk-1*(*ne2257*ts); *src-1* (*RNAi*) embryos to levels characteristic of *src-1*–depleted embryos (Fig. 5*A* and Table S1). Taken together, these results indicate that CDK-1 functions along with Wnt signaling to regulate WRM-1 localization and the EMS division axis.

Discussion

Wnt signaling in *C. elegans* contributes to endoderm specification and orientation of the division axis of the four-cell stage endo-

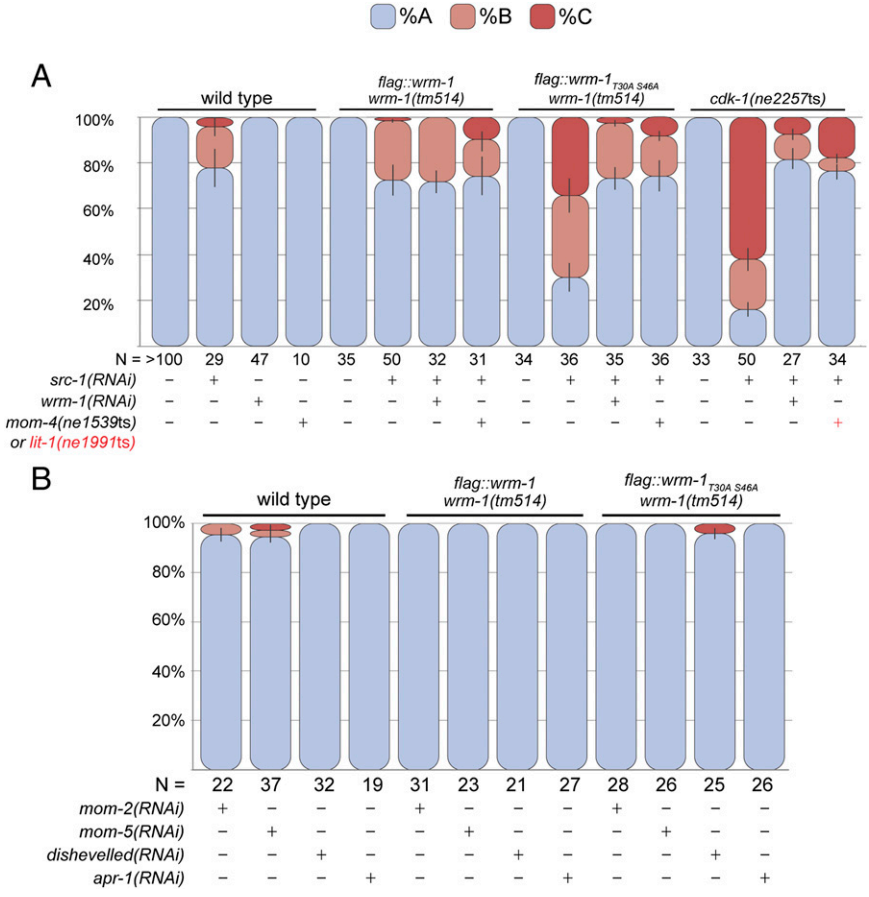

Fig. 5. Polarity defect in *cdk-1* mutants is rescued by removal of cortical WRM-1. (*A*) Stacked bar graphs as in Fig. 2. *src-1*(*RNAi*)-dependent spindle rotation defect in the transgenic line harboring *flag::wrm-1*$_{T30AS46A}$ and *cdk-1*(*ne2257*ts) mutant grown at 20 °C is rescued in animals further subjected to *wrm-1*(*RNAi*) or animals containing *mom-4(ne1539*ts*) or lit-1(ne1539*ts*)* mutations (+ in red). (*B*) Synergistic effect on the spindle rotation defect is not observed when the transgenic line harboring *flag::wrm-1*$_{T30AS46A}$ is treated with *RNAi* targeting Wnt signaling components *mom-2, mom-5, disheveled*, or *apr-1*. N represents the number of embryos scored.

derm precursor EMS. Upstream Wnt/Frizzled components act through WRM-1/β-catenin to specify endoderm, whereas EMS division orientation is achieved independently of WRM-1 activity (16, 18, 19). Our data suggest that Wnt-signaling factors and CDK-1 promote the release of cortical WRM-1, which facilitates EMS spindle rotation by exposing an intrinsic polarity cue.

Redundancy and Robustness in P2/EMS Signaling. *C. elegans* embryos exhibit a surprising degree of redundancy in both endoderm induction and control of EMS division orientation. For example, double-mutant animals homozygous for presumptive null alleles of the upstream Wnt-signaling components *mom-2/wnt* and *mom-5/frizzled* produce embryos in which EMS is properly specified greater than 90% of the time. Similarly, although rotation is delayed in upstream Wnt-signaling mutants (17, 19), EMS ultimately orients with a WT a-p division axis in nearly 100% of cases. Null alleles or RNAi of Src-signaling components result in embryos in which endoderm is always specified properly and EMS divides with a WT a-p orientation in >70% of cases. Strikingly, double-mutant combinations between Wnt- and Src-signaling components exhibit a fully penetrant defect in both endoderm specification and EMS division orientation (15).

We have shown here that depletion of cortical WRM-1 can suppress the penetrant EMS a-p division orientation defect of Wnt and Src double mutants, suggesting that the removal of WRM-1 uncovers a ground state a-p polarity signal that is independent of both Wnt and Src signaling. This ground-state signal may represent a remnant of the initial a-p polarity cue established at fertilization. For example, earlier studies have shown that, in the absence of Src signaling, P2 responds to an underlying a-p polarity cue (15). WT P2 produces a smaller anterior daughter, P3, which inherits the germ-line nuage-like structures called P-granules. In Src-signaling mutants, however, P2 exhibits a reversed polarity and instead, produces a smaller posterior daughter, which inherits the P-granules (15). Interestingly, in the parasitic nematode *Acrobeloides nanus*, P2 produces P3 on its posterior rather than anterior side (34), which is identical to the phenotype observed in *C. elegans* Src-signaling mutants. Thus, in *A. nanus* and *C. elegans* Src-pathway mutants, P2 exhibits the same a-p polarity as its progenitors P0 and P1. Assuming that this phenotype represents an ancestral state, Src signaling in *C. elegans* may have evolved to reverse the polarity of P2 and thus, bypass the need for migration of P3 and its descendants. These findings support the idea that, in the absence of Wnt and Src signaling, both EMS and P2 respond to an intrinsic a-p polarity cue.

Previous work has shown that the PAR proteins are required for an intrinsic mechanism that orients the spindle in asymmetrically dividing cells (8). In nonpolarized cells, however, PAR-3 prevents spindle rotation that is driven by geometric asymmetry caused by cell shape (27). For example, in two-cell *par-3* mutant embryos, the nuclear–centrosome complex in each blastomere (AB and P1) always rotates to the flat surface at the cell contact. Analogous to PAR-3, WRM-1 may be involved in preventing EMS from responding to geometric asymmetry until the polarity signal from P2 overrides it.

CDK-1 and Wnt Signaling Are Required for WRM-1 Cortical Release. During the EMS cell cycle, the mitotic apparatus is initially set up on the l-r axis of the embryo. Later, during mitotic prophase, astral microtubules from one pole seem to capture the posterior cortex of the cell and rotate the EMS spindle onto the a-p axis (35). The cortical release of WRM-1 at prophase coincides with the timing of astral–cortical capture in EMS and thus, may be timed to unmask a cortical cell polarity cue that promotes rotation of the nascent EMS spindle (Fig. 6). The finding that WRM-$1_{T30A\ S46A}$ is retained at the cortex suggests that modification by CDK-1 may help restrict the timing of WRM-1 cortical release to the appropriate time in the EMS cell cycle. Consistent with this possibility, we have shown that a hypomorphic allele of *cdk-1* exhibits defects in WRM-1 cortical release identical to the defects observed in WRM-$1_{T30A\ S46A}$ transgenic animals. Taken together, these findings suggest that phosphorylation of WRM-1 by CDK-1 is necessary for WRM-1 cortical release, and these findings are consistent with a model in which CDK-1 primes WRM-1 for cortical release in response to Wnt signaling.

We have shown that WRM-$1_{T30A\ S46A}$ remains cortical and inhibits rotation of EMS spindle as well as nuclear accumulation of WRM-1 in early embryogenesis. Our findings are consistent with a previous study showing that, when artificially tethered to the cortex, WRM-1 inhibits Wnt signaling and nuclear localization of WRM-1 in postembryonic cells (36). These results support the conclusion that asymmetric cortical WRM-1 is required to establish nuclear asymmetry of WRM-1. Recent work has suggested the molecular mechanism by which cortical WRM-1 regulates nuclear asymmetry of WRM-1 (37). Cortical release of WRM-1 induced by Wnt signaling establishes both asymmetric cortical localization of APR-1 (Adenomatous polyposis coli-related 1) and asymmetric distribution of astral microtubules, with more microtubules on the anterior side of EMS. Kinesin-dependent nuclear export of WRM-1, in turn, creates asymmetric nuclear localization of WRM-1 (37). Based on these findings, it was proposed that asymmetric nuclear WRM-1 is required for the endoderm induction. Surprisingly, we found that endoderm induction was nearly WT in worms expressing WRM-$1_{T30A\ S46A}$, despite its cortical retention and reduced nuclear asymmetry. Our findings suggest that, in addition to the observed physical asymmetries in WRM-1 localization, polarity signaling in the early embryo must also generate functional asymmetries in WRM-1 activity. For example, WRM-1 activity in the nucleus seems to be dependent on LIT-1 kinase activity, and a low level of nuclear LIT-1 is enriched in the E, but not the MS, blastomere (38). Therefore, it remains possible that

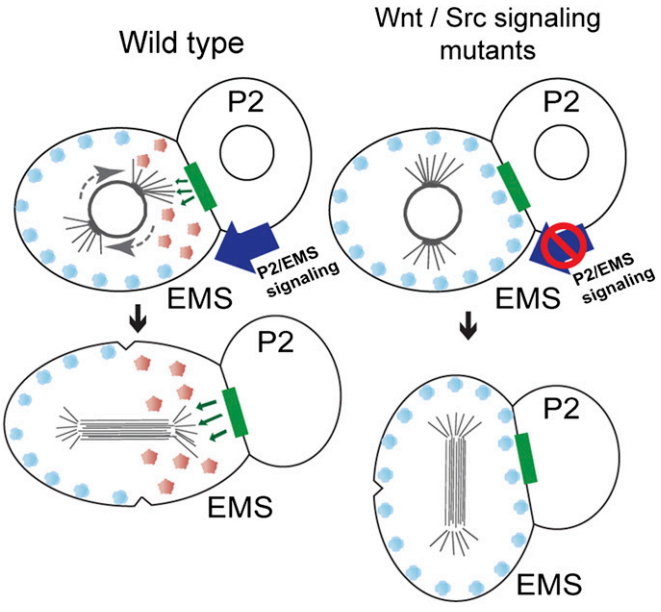

Fig. 6. WRM-1 as a masking factor in EMS polarity. In the WT embryo, Wnt and CDK-1 regulate the release of WRM-1 protein from the cortex, unmasking an intrinsic polarity cue(s) necessary to rotate the EMS spindle onto the a-p axis. In Wnt-signaling mutants or CDK-1 phosphoacceptor site mutants, WRM-1 protein is retained at the cortex. This cortical WRM-1 interferes with the reorientation of the EMS spindle (l-r) when Src signaling is impaired. Removing WRM-1 protein in these mutant backgrounds results in a partial return to EMS a-p polarity. Inherent polarity cues, green rectangles; phosphorylated WRM-1, red circles; WRM-1, blue circles.

asymmetric activity of the LIT-1/WRM-1 kinase between the daughters of EMS promotes endoderm differentiation in *wrm-1*$_{T30A\ S46A}$ rescue worms.

Downstream of P2/EMS Signaling in Cell Polarity. An important question that remains is whether CDK-1 targets WRM-1 in a signal-dependent manner—for example, by only phosphorylating a subpopulation of WRM-1 on the membrane proximal to the P2/EMS contact site. Previous reports suggest that Wnt induces Frizzled to interact at the membrane with its coreceptor Low density lipoprotein receptor-related protein 6, LRP6 (39–41). This complex recruits Dishevelled, which in turn, induces GSK3β and CK1γ-dependent phosphorylation of LRP6 (42, 43). Although an LRP6-like coreceptor has not been identified in *C. elegans*, Frizzled and Dishevelled have been reported to accumulate at the Wnt-responsive cortex of postembryonic cells (36, 44–46) and in the case of Dishevelled, the boundary of P2 and EMS cells (18, 47). Perhaps a similar signal-induced complex modifies cortical WRM-1 at the P2/EMS junction to permit subsequent recognition by CDK-1 at the appropriate time in the cell cycle.

Independent of Wnt signaling, the receptor tyrosine kinase-related protein MES-1 localizes at the P2/EMS contact site and activates cortical SRC-1 (15). Thus, both Wnt- and Src-signaling components are present and activated at the P2/EMS cortex. The finding that WRM-1$_{T30A\ S46A}$ synergizes with *src-1*, but not Wnt-pathway mutants, suggests that modification by CDK-1 governs the cortical release of WRM-1 in response to Wnt-signaling cues, whereas SRC-1 may independently regulate WRM-1 or some other associated cortical factor(s) to promote EMS spindle rotation. Consistent with this model, the G protein regulators Gα (GPR-1/-2) and LET-99 were shown to asymmetrically localize at the cortex and orient the EMS spindle in response to Src, but not Wnt, signaling (48–50). LET-99 is also required for the geometry-driven spindle rotation in *par-3* mutant embryos (27). It will be interesting to test whether the geometric asymmetry of EMS cell orients the spindle along the a-p axis in a *mom-2; src-1; wrm-1* triple mutant and if so, whether spindle rotation depends on LET-99 activity.

In summary, we have shown that Wnt signaling and CDK-1–dependent phosphorylation influence the EMS cell division axis by regulating the cortical release of WRM-1/β-catenin. Cell cycle regulation of Wnt signaling seems to be evolutionally conserved. In vertebrates, cytoplasmic β-catenin levels oscillate during the cell cycle in synchronized epithelial cells (51). Other studies suggest that the stability of cytoplasmic β-catenin is directly regulated by CDK6/cyclin D complexes (52, 53), whereas the mitotic CDK14/cyclin Y complexes promote Wnt signaling by phosphorylating the LRP6 coreceptor (54). *C. elegans* embryos undergo rapid cell division and patterning simultaneously. Because there is little time for misaligned cells to migrate into the correct position, the orientation of asymmetric divisions must be tightly coupled to both the cell cycle and cellular and organismal polarity. Here, we have shown that CDK-1 directly phosphorylates WRM-1/β-catenin to facilitate this process during P2/EMS signaling. In the future, it will be interesting to explore what other pathways couple cell division and cell fate and whether the underlying mechanisms are conserved.

Materials and Methods

Microscopy. GFP::WRM-1 embryos were mounted in dH_2O on RITE-ON glass slides (Beckton Dickinson). Epifluorescence and differential interference contrast (DIC) microscopy were performed using an Axioplan2 Microscope (Zeiss). Images were captured using an ORCA-ER digital camera (Hamamatsu) and OPENLAB (Improvision) software. 2D deconvolution of GFP images was performed in MetaMorph (Molecular Devices), version 7.6.6, with the following settings: XY spacing = 0.11, Z spacing = 0.50, N.A. = 1.40, refractive index = 1.515, wavelength = 530, and filter size = 22.

Phenotypic Analysis of the Orientation of Cell Division Axis. Embryos were mounted on 2% (wt/vol) agarose pads and examined under DIC microscopy. The orientation of EMS cell division axis was scored at the late four-cell stage and categorized according to the angle of the mitotic spindle relative to the a-p axis of the embryo as the cytokinesis occurs.

Category A. The angle of the mitotic spindle relative to the a-p axis at cytokinesis is between 0° and 45°. The mitotic spindle is set up either along the a-p or in a skewed a-p orientation as seen in the majority of *src-1* single-mutant embryos. At the end of EMS cell division, only one daughter cell is touching the P2 cell.

Category B. The angle relative to the a-p axis at cytokinesis is greater than 45° but less than 90°. The mitotic spindle is set up perpendicular to the focal plane, and both EMS daughter cells touch the P2 cell.

Category C. The mitotic spindle is set up perpendicular to the focal plane, the angle relative to the a-p axis at cytokinesis is 90°, and both EMS daughter cells touch the P2 cell. The score is based on the terminal phenotype, and the slight delay of spindle rotation seen in some of the *wnt* and *src-1* mutants is not considered; *mes-1* phenotype was scored at 25 °C.

Cell Culture and Transfection. 293T cells were grown in DMEM supplemented with 10% (vol/vol) FBS on a 35-mm dish. Transient transfections were performed using Effectene reagent (QIAGEN) according to the manufacturer's instructions.

Immunoprecipitation and in Vitro Kinase Assays. Transfected cells were harvested 24 h posttransfection and lysed in 750 μL lysis buffer (50 mM Tris·HCl, pH 7.4, 150 mM NaCl, 1% (vol/vol) Nonidet P-40, 1 mM DTT, 50 mM β-glycerophosphate, 1 mM sodium orthovanadate, 0.05 mM sodium fluoride, 1 mM PMSF supplemented with Complete mini Protease Inhibitors, EDTA-free; Roche). Immunoprecipitation of FLAG::LIT-1 protein from 293T cells was performed using anti-FLAG M2-Agarose (Sigma). Immune complexes were washed three times with the lysis buffer and one time with kinase buffer (50 mM Hepes, pH 7.4, 10 mM $MgCl_2$, 10 mM DTT, 0.5 mM NaF, 0.1 mM sodium orthovanadate, 5 μg/mL leupeptin), and then, it was divided for kinase assays. In vitro kinase assays were performed in 25 μL (final volume) kinase buffer containing substrate (20 ng/μL) and 0.04 μCi/μL γ-[^{32}P]ATP (6,000 Ci/mmol; Amersham) for 15 min at 25 °C. After the kinase reaction, immune complexes were pelleted at 20,000 × *g*, and supernatants containing the substrate were transferred to fresh tubes. Pellets containing the immune complex were denatured and subjected to SDS/PAGE followed by autoradiography. GST substrates were recovered from the supernatant by adding 500 μL binding buffer [0.5% (vol/vol) Nonidet P-40, 50 mM Tris·HCl, pH 8.5, 100 mM NaCl, 1 mM EDTA, 1 mM DTT, 1 mM PMSF] supplemented with Phosstop phosphatase inhibitors (Roche) and Complete Mini Protease inhibitors, EDTA-free (Roche) and glutathione-Sepharose (GE) beads. After rotating at 4 °C for 1 h, the beads were washed three times with the binding buffer and one time with water. GST complexes were denatured and analyzed by SDS/PAGE and autoradiography.

Worm CDK-1 kinase activity was measured as described previously (33). For immunoprecipitation of endogenous CDK-1 complexes, ~3.5×10^6 embryos were suspended in 2 mL lysis buffer and homogenized in a one-shot cell disruptor (Cell Disruption Systems). The lysate was cleared by centrifugation at 20,000 × *g* and incubated with anti–CYB-1 or anti–CYB-3 antisera for 1 h at 4 °C. Immune complexes were captured on protein A Sepharose beads (Amersham Pharmacia) with rotation at 4 °C for 1 h. Immune complexes were washed three times with the lysis buffer and one time with the kinase buffer and then divided for kinase assays.

CDK1/GSK3β sequential kinase assay were performed by preincubating substrate GST-fusion proteins (20 ng/μL) with 2 ng/μL vertebrate CDC2/Cyclin B (NEB) in the presence of 100 μM nonradiolabeled ATP in kinase buffer (final volume of 25 μL) at 25 °C for 30 min. Substrates were then immobilized on glutathione-Sepharose beads and washed three times with the binding buffer and one time with the kinase buffer. GST complexes were resuspended in 25 μL kinase buffer containing 2 ng/μL vertebrate GSK3β (NEB) and 0.04 μCi/μL γ-[^{32}P]ATP and incubated at 25 °C for 15 min. Reactions were analyzed by SDS and autoradiography as described above. The following plasmids were used to express WRM-1 or POP-1 GST-fusion substrates for in vitro kinase assays: B1224, GST-WRM-1(1–140); B1337, GST-WRM-1(1-140, T30A); B1338, GST-WRM-1(1-140, S46A); B1339, GST-WRM-1(1-140, T30A; S46A); and B1360, GST-POP-1(1-188).

GSK-3 Spot Assay. WRM-1 peptides [WT, MTPSTSRVSTPVR; phospho-WT, MTPSTSRVS(pT)PVR; phospho-S26A, MTPSTARVS(pT)PVR] were obtained from Genscript. *C. elegans* GSK-3 was expressed and purified from *Escherichia coli*. The kinase reactions were performed in 25 μL (final volume) kinase

buffer containing ATP (50 μM), γ-[^{32}P]ATP (0.16 μCi/μL), substrate peptide (400 ng/mL), and recombinant *C. elegans* GSK-3 (4 ng/μg) at 25 °C for 20 min. Reactions were terminated by spotting 20 μL reaction mixtures on p81 phosphocellulose paper squares (Upstate). The paper was air dried, washed three times with 1% (vol/vol) phosphoric acid, and transferred to scintillation tubes containing Opti-Fluor scintillation mixture (Perkin-Elmer). Radioactivity was counted in a scintillation counter (Beckton Coulter).

Generation of Transgenic Lines Expressing GFP Fusion Proteins. The *gfp::wrm-1* transgenic strain was described previously (21). To express *gfp*::*wrm-1* with various mutations in vivo, the genomic fragment from SpeI and BglII sites (5.7 kb) containing the entire *wrm-1* coding sequence was cloned from cosmid T16E10 and inserted into Bluescript KS(+). A BglII site was created by site-directed mutagenesis behind the first translation initiation codon (ATG) of the *wrm-1* gene. The *gfp* sequence from pPD95.75 was amplified by PCR, digested with BamHI, and inserted into the BglII site. The CDK-1 (T30 and S46) and GSK-3 (S26A) phosphoacceptor mutations were introduced by site-directed mutagenesis. Microparticle bombardment (30) was used to generate the transgenes *neIs15* [*gfp*::*wrm-1* $_{T30A\ S46A}$, *unc-119*(+)], *neIs24* [*gfp*::*wrm-1* $_{T30D\ S46D}$, *unc-119*(+)], and *neIs16* [*gfp::wrm-1*$_{S26A}$, *unc-119*(+)].

Generation of MosSCI Transgenes. A 7.5-kb genomic DNA fragment (from BstZ171 to BglII sites) containing *wrm-1*, with or without mutations in CDK-1 phosphoacceptor sites, was inserted into a modified version of pCFJ151 vector (31). The 3x flag sequence (GATTACAAAGACCATGATGGTGACTATAAGGATCATGATATTGACTATAAAGACGATGACGATAAG) was inserted in the BglII site created by site-directed mutagenesis behind the first initiation codon of *wrm-1* gene. The *wrm-1* constructs were present at 1–2 ng/μL in the injection mixture for the MosSCI direct insertion method (31). At concentrations higher than 5 ng/μL, the *wrm-1* constructs were toxic. On average, one integration line was obtained per 100 injected animals. For each construct, we obtained at least two independent lines, and proper single-copy insertion was confirmed by PCR and DNA sequence for all lines. Each line expressed an equal level of WRM-1 protein as determined by immunoblot, with FLAG antibodies using extract prepared from worm embryos. The following MosSCI transgenes were used in this study: *neSi3*[*flag*::*wrm-1*, *cb-unc-119(+)*]II, *neSi4*[*flag*:: *wrm-1*$_{T30A\ S46A}$, *cb-unc-119(+)*]II, *neSi5*[*wrm-1*, *cb-unc-119(+)*]II, and *neSi6*[*wrm-1*$_{T30A\ S46A}$, *cb-unc-119(+)*]II.

ACKNOWLEDGMENTS. The authors thank members of the C.C.M. laboratory for useful discussions. We are grateful to Dr. Agata Jurczyk for help in processing micrographic images, Dr. Tuba Bas for initial technical help, Dr. Sander van den Heuvel for CYB-1 and CYB-3 antibodies, and Dr. Rueyling Lin for the *gfp*::*oma-1* strain. This work was supported by National Institutes of Health Grants GM081670 (to M.C.S.) and HD36247 (to C.C.M.). C.C.M. is a Howard Hughes Medical Institute Investigator.

1. Horvitz HR, Herskowitz I (1992) Mechanisms of asymmetric cell division: Two Bs or not two Bs, that is the question. *Cell* 68(2):237–255.
2. Ahringer J (2003) Control of cell polarity and mitotic spindle positioning in animal cells. *Curr Opin Cell Biol* 15(1):73–81.
3. Gong Y, Mo C, Fraser SE (2004) Planar cell polarity signalling controls cell division orientation during zebrafish gastrulation. *Nature* 430(7000):689–693.
4. Chia W, Somers WG, Wang H (2008) Drosophila neuroblast asymmetric divisions: Cell cycle regulators, asymmetric protein localization, and tumorigenesis. *J Cell Biol* 180(2): 267–272.
5. Goldstein B, Hird SN (1996) Specification of the anteroposterior axis in Caenorhabditis elegans. *Development* 122(5):1467–1474.
6. Rose LS, Kemphues KJ (1998) Early patterning of the C. elegans embryo. *Annu Rev Genet* 32:521–545.
7. Cowan CR, Hyman AA (2004) Asymmetric cell division in C. elegans: Cortical polarity and spindle positioning. *Annu Rev Cell Dev Biol* 20:427–453.
8. Cheng NN, Kirby CM, Kemphues KJ (1995) Control of cleavage spindle orientation in Caenorhabditis elegans: The role of the genes par-2 and par-3. *Genetics* 139(2): 549–559.
9. Etemad-Moghadam B, Guo S, Kemphues KJ (1995) Asymmetrically distributed PAR-3 protein contributes to cell polarity and spindle alignment in early C. elegans embryos. *Cell* 83(5):743–752.
10. Nance J, Priess JR (2002) Cell polarity and gastrulation in C. elegans. *Development* 129(2):387–397.
11. Goldstein B (1992) Induction of gut in Caenorhabditis elegans embryos. *Nature* 357(6375):255–257.
12. Goldstein B (1993) Establishment of gut fate in the E lineage of C. elegans: The roles of lineage-dependent mechanisms and cell interactions. *Development* 118(4): 1267–1277.
13. Goldstein B (1995) An analysis of the response to gut induction in the C. elegans embryo. *Development* 121(4):1227–1236.
14. Goldstein B (1995) Cell contacts orient some cell division axes in the Caenorhabditis elegans embryo. *J Cell Biol* 129(4):1071–1080.
15. Bei Y, et al. (2002) SRC-1 and Wnt signaling act together to specify endoderm and to control cleavage orientation in early C. elegans embryos. *Dev Cell* 3(1):113–125.
16. Rocheleau CE, et al. (1997) Wnt signaling and an APC-related gene specify endoderm in early C. elegans embryos. *Cell* 90(4):707–716.
17. Thorpe CJ, Schlesinger A, Carter JC, Bowerman B (1997) Wnt signaling polarizes an early C. elegans blastomere to distinguish endoderm from mesoderm. *Cell* 90(4): 695–705.
18. Walston T, et al. (2004) Multiple Wnt signaling pathways converge to orient the mitotic spindle in early C. elegans embryos. *Dev Cell* 7(6):831–841.
19. Schlesinger A, Shelton CA, Maloof JN, Meneghini M, Bowerman B (1999) Wnt pathway components orient a mitotic spindle in the early Caenorhabditis elegans embryo without requiring gene transcription in the responding cell. *Genes Dev* 13(15):2028–2038.
20. Mizumoto K, Sawa H (2007) Two betas or not two betas: Regulation of asymmetric division by beta-catenin. *Trends Cell Biol* 17(10):465–473.
21. Nakamura K, et al. (2005) Wnt signaling drives WRM-1/beta-catenin asymmetries in early C. elegans embryos. *Genes Dev* 19(15):1749–1754.
22. Takeshita H, Sawa H (2005) Asymmetric cortical and nuclear localizations of WRM-1/beta-catenin during asymmetric cell division in C. elegans. *Genes Dev* 19(15): 1743–1748.
23. Browning H, et al. (1996) Macrorestriction analysis of Caenorhabditis elegans genomic DNA. *Genetics* 144(2):609–619.
24. Meneghini MD, et al. (1999) MAP kinase and Wnt pathways converge to downregulate an HMG-domain repressor in Caenorhabditis elegans. *Nature* 399(6738):793–797.
25. Rocheleau CE, et al. (1999) WRM-1 activates the LIT-1 protein kinase to transduce anterior/posterior polarity signals in C. elegans. *Cell* 97(6):717–726.
26. Shin TH, et al. (1999) MOM-4, a MAP kinase kinase kinase-related protein, activates WRM-1/LIT-1 kinase to transduce anterior/posterior polarity signals in C. elegans. *Mol Cell* 4(2):275–280.
27. Tsou MF, Ku W, Hayashi A, Rose LS (2003) PAR-dependent and geometry-dependent mechanisms of spindle positioning. *J Cell Biol* 160(6):845–855.
28. Wildwater M, Sander N, de Vreede G, van den Heuvel S (2011) Cell shape and Wnt signaling redundantly control the division axis of C. elegans epithelial stem cells. *Development* 138(20):4375–4385.
29. Obenauer JC, Cantley LC, Yaffe MB (2003) Scansite 2.0: Proteome-wide prediction of cell signaling interactions using short sequence motifs. *Nucleic Acids Res* 31(13):3635–3641.
30. Praitis V (2006) Creation of transgenic lines using microparticle bombardment methods. *Methods Mol Biol* 351:93–107.
31. Frøkjaer-Jensen C, et al. (2008) Single-copy insertion of transgenes in Caenorhabditis elegans. *Nat Genet* 40(11):1375–1383.
32. Boxem M, Srinivasan DG, van den Heuvel S (1999) The Caenorhabditis elegans gene ncc-1 encodes a cdc2-related kinase required for M phase in meiotic and mitotic cell divisions, but not for S phase. *Development* 126(10):2227–2239.
33. Shirayama M, et al. (2006) The Conserved Kinases CDK-1, GSK-3, KIN-19, and MBK-2 Promote OMA-1 Destruction to Regulate the Oocyte-to-Embryo Transition in C. elegans. *Curr Biol* 16(1):47–55.
34. Skiba F, Schierenberg E (1992) Cell lineages, developmental timing, and spatial pattern formation in embryos of free-living soil nematodes. *Dev Biol* 151(2):597–610.
35. Goldstein B (2000) When cells tell their neighbors which direction to divide. *Dev Dyn* 218(1):23–29.
36. Mizumoto K, Sawa H (2007) Cortical beta-catenin and APC regulate asymmetric nuclear beta-catenin localization during asymmetric cell division in C. elegans. *Dev Cell* 12(2):287–299.
37. Sugioka K, Mizumoto K, Sawa H (2011) Wnt regulates spindle asymmetry to generate asymmetric nuclear β-catenin in C. elegans. *Cell* 146(6):942–954.
38. Lo MC, Gay F, Odom R, Shi Y, Lin R (2004) Phosphorylation by the beta-catenin/MAPK complex promotes 14-3-3-mediated nuclear export of TCF/POP-1 in signal-responsive cells in C. elegans. *Cell* 117(1):95–106.
39. Pinson KI, Brennan J, Monkley S, Avery BJ, Skarnes WC (2000) An LDL-receptor-related protein mediates Wnt signalling in mice. *Nature* 407(6803):535–538.
40. Tamai K, et al. (2000) LDL-receptor-related proteins in Wnt signal transduction. *Nature* 407(6803):530–535.
41. Wehrli M, et al. (2000) arrow encodes an LDL-receptor-related protein essential for Wingless signalling. *Nature* 407(6803):527–530.
42. Bilic J, et al. (2007) Wnt induces LRP6 signalosomes and promotes dishevelled-dependent LRP6 phosphorylation. *Science* 316(5831):1619–1622.
43. Zeng X, et al. (2005) A dual-kinase mechanism for Wnt co-receptor phosphorylation and activation. *Nature* 438(7069):873–877.
44. Goldstein B, Takeshita H, Mizumoto K, Sawa H (2006) Wnt signals can function as positional cues in establishing cell polarity. *Dev Cell* 10(3):391–396.
45. Park FD, Tenlen JR, Priess JR (2004) C. elegans MOM-5/frizzled functions in MOM-2/Wnt-independent cell polarity and is localized asymmetrically prior to cell division. *Curr Biol* 14(24):2252–2258.
46. Wu M, Herman MA (2007) Asymmetric localizations of LIN-17/Fz and MIG-5/Dsh are involved in the asymmetric B cell division in C. elegans. *Dev Biol* 303(2):650–662.

47. Hawkins NC, Ellis GC, Bowerman B, Garriga G (2005) MOM-5 frizzled regulates the distribution of DSH-2 to control C. elegans asymmetric neuroblast divisions. *Dev Biol* 284(1):246–259.
48. Tsou MF, Hayashi A, Rose LS (2003) LET-99 opposes Galpha/GPR signaling to generate asymmetry for spindle positioning in response to PAR and MES-1/SRC-1 signaling. *Development* 130(23):5717–5730.
49. Srinivasan DG, Fisk RM, Xu H, van den Heuvel S (2003) A complex of LIN-5 and GPR proteins regulates G protein signaling and spindle function in C elegans. *Genes Dev* 17(10):1225–1239.
50. Werts AD, Roh-Johnson M, Goldstein B (2011) Dynamic localization of C. elegans TPR-GoLoco proteins mediates mitotic spindle orientation by extrinsic signaling. *Development* 138(20):4411–4422.
51. Olmeda D, Castel S, Vilaró S, Cano A (2003) Beta-catenin regulation during the cell cycle: Implications in G2/M and apoptosis. *Mol Biol Cell* 14(7):2844–2860.
52. Park CS, et al. (2004) Modulation of beta-catenin phosphorylation/degradation by cyclin-dependent kinase 2. *J Biol Chem* 279(19):19592–19599.
53. Park CS, et al. (2007) Modulation of beta-catenin by cyclin-dependent kinase 6 in Wnt-stimulated cells. *Eur J Cell Biol* 86(2):111–123.
54. Davidson G, et al. (2009) Cell cycle control of wnt receptor activation. *Dev Cell* 17(6):788–799.

Supporting Information

Kim et al. 10.1073/pnas.1300769110

SI Results

RNAi of *pop-1* (*posterior pharynx defect 1*) and *apr-1* (*adenomatous polyposis coli-related 1*), which are thought to be downstream Wingless/int (Wnt)/β-catenin–related signaling factors, resulted in fully penetrant embryonic lethality but had no affect on WRM-1 (Worm armadillo 1) cortical release (Fig. S1 *A* and *F*). However, in both mutants, WRM-1 nuclear accumulation was significantly reduced (Fig. S2 *A* and *G*), suggesting that these factors promote the nuclear accumulation of WRM-1 downstream of its cortical release. Especially in *apr-1*(*RNAi*), as previously observed (1), the nuclear WRM-1 levels were globally reduced in all cells in the two-, four-, and eight-cell stages, suggesting a general role for APR-1 in WRM-1 nuclear accumulation (Fig. S2*A*). In post-embryonic cells, WRM-1 accumulates in both nuclei of T daughter cells after it is released from the posterior cortex in *apr-1* mutants (2); therefore, APR-1 may have opposite function in terms of nuclear retention of WRM-1 in the endomesoderm (EMS) blastomere and T cells.

RNAi of *glycogen synthase kinase 3* (*gsk-3*) causes cortical retention of WRM-1 as in other upstream Wnt signaling mutants (Fig. 1*C*). However, the interpretation of this phenotype is complicated by the fact that *gsk-3*(*RNAi*) or *gsk-3* deletion allele (*nr2047*) causes an ectopic stabilization of the Oocyte maturation defective 1 gene product, OMA-1 (3). Because WRM-1 is retained on the EMS cortex when OMA-1 is misregulated (Figs. S1 *D* and *F* and S2 *D* and *G*), we cannot exclude the possibility that cortical regulation of WRM-1 by GSK-3 is indirect through stabilized OMA-1 without additional analysis.

1. Nakamura K, et al. (2005) Wnt signaling drives WRM-1/beta-catenin asymmetries in early C. elegans embryos. *Genes Dev* 19(15):1749–1754.
2. Mizumoto K, Sawa H (2007) Cortical beta-catenin and APC regulate asymmetric nuclear beta-catenin localization during asymmetric cell division in C. elegans. *Dev Cell* 12(2):287–299.
3. Shirayama M, et al. (2006) The conserved kinases CDK-1, GSK-3, KIN-19, and MBK-2 promote OMA-1 destruction to regulate the oocyte-to-embryo transition in C. elegans. *Curr Biol* 16(1):47–55.

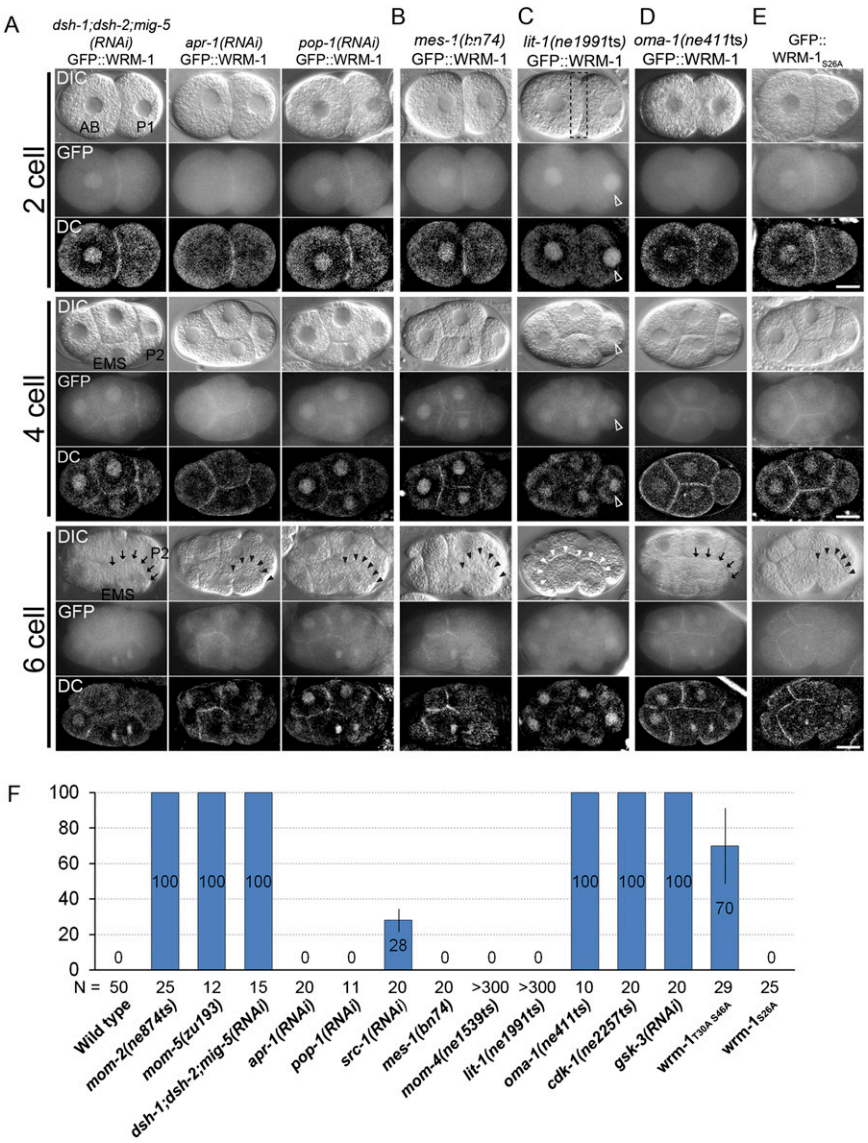

Fig. S1. WRM-1 localization in two-, four-, and six-cell stage embryos. (*A–E*) Nomarski (DIC), fluorescence (GFP), and deconvoluted fluorescence (DC) micrographs of two-, four-, and six-cell stage embryos in the genetic backgrounds indicated. Black arrowheads indicate posterior cortex of dividing EMS cell where the cortical WRM-1 is absent as in WT (Fig. 1*A*). A departure from WT localization pattern is indicated as follows: black arrows, posterior EMS cortex with cortical WRM-1 retention; dotted box, absence of cortical WRM-1 at AB and P1 boundary; empty arrowheads, accumulation of abnormal nuclear WRM-1 in P1 and P2 blastomeres; white arrowheads, entire EMS cortex without cortical WRM-1 localization. Anterior is to the left, and dorsal is up. (Scale bar: 10 μm.) (*F*) Quantification of cortical WRM-1 asymmetry during EMS division. Percentage of embryos that abnormally retain WRM-1 at the posterior cortex during EMS cell division is shown. Genotypes and the number of embryos scored (N) are indicated at the bottom of each bar graph.

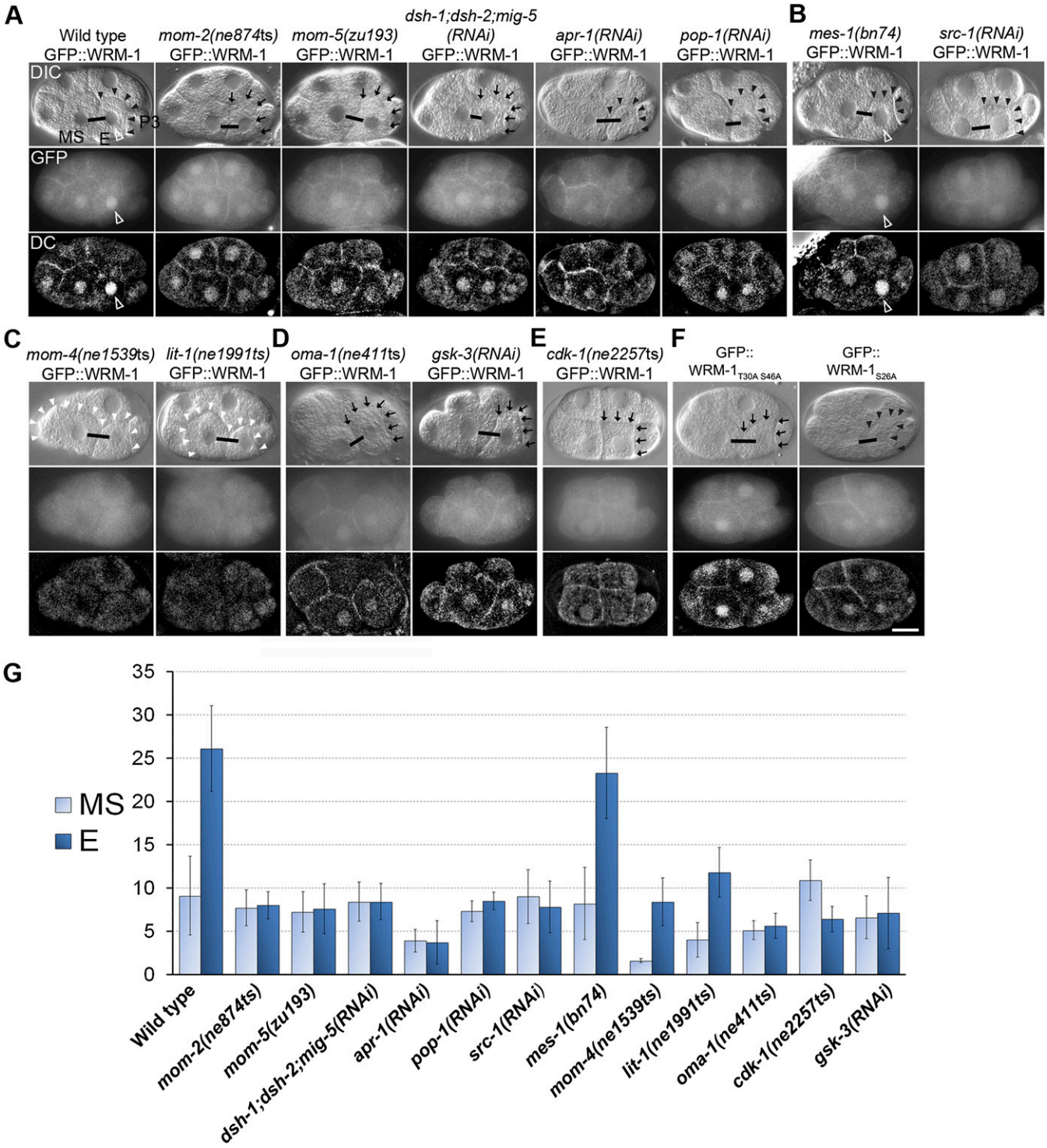

Fig. S2. WRM-1 localization in eight-cell stage embryos. (*A–F*) Nomarski (DIC), fluorescence (GFP), and deconvoluted fluorescence (DC) micrographs of eight-cell stage embryos in the genetic backgrounds indicated. In WT embryos, WRM-1 accumulates to a higher level in the nucleus of E (empty arrowheads) and is absent from the posterior cortex of E (black arrowheads). A departure from the WT localization pattern is indicated as follows: black arrows, WRM-1 is retained at the cortex of E; white arrowheads, WRM-1 is missing from the entire cortex of both E and MS. Black lines connect the nuclei of EMS daughters MS and E. Anterior is to the left, and dorsal is up. (Scale bar: 10 μm.) (*G*) Quantification of nuclear WRM-1 localization in MS and E cells from eight-cell stage embryos. Relative signal intensity of nuclear GFP::WRM-1 in MS and E cells of eight-cell embryos in various genetic backgrounds is shown as indicated. Average signal intensity of 10 embryos from each genotype was analyzed using ImageJ software, in which the nuclear signal value was normalized to the signal in the cytoplasm. Error bars indicate SD.

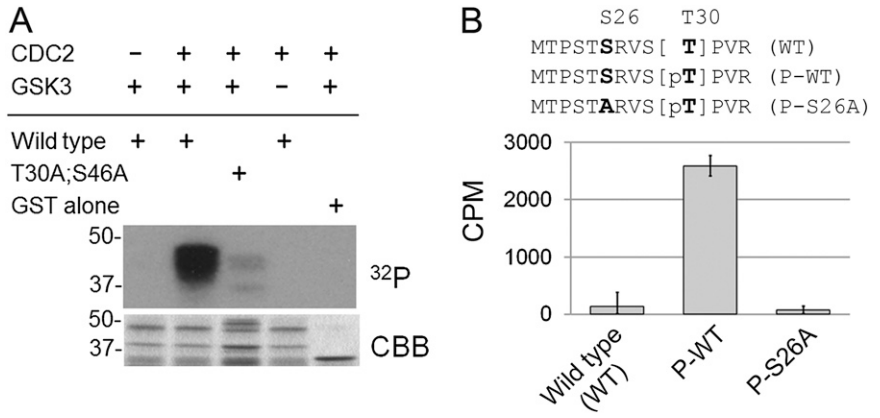

Fig. S3. Sequential phosphorylation of WRM-1 by CDK-1 and GSK-3. (*A*) WT [GST-WRM-1(1-140)], T30A;S46A [GST-WRM-1(1-140) with CDK-phosphoacceptor mutations], or GST alone were incubated first with nonradiolabeled ATP in the presence or absence of human CDC2/cyclin B complex (indicated by CDC2 + or −). After extensive washing, substrates were incubated with γ-[^{32}P]ATP in the presence or absence of vertebrate GSK3β (indicated by GSK3 + or −). Substrates were fractionated by SDS/PAGE and stained with Coomassie Brilliant Blue (CBB). Autoradiography was performed to detect phosphorylation products (^{32}P). (*B*) Recombinant *Caenorhabditis elegans* GSK-3 was used to phosphorylate synthetic WRM-1 peptides encompassing the conserved GSK-3 (S26) and CDK-1(T30) phosphoacceptor sites as indicated with (P-WT) or without (WT) the priming phosphorylation at T30 and with a Ser to Ala mutation at S26 in addition to the priming phosphorylation at T30 (P-S26A).

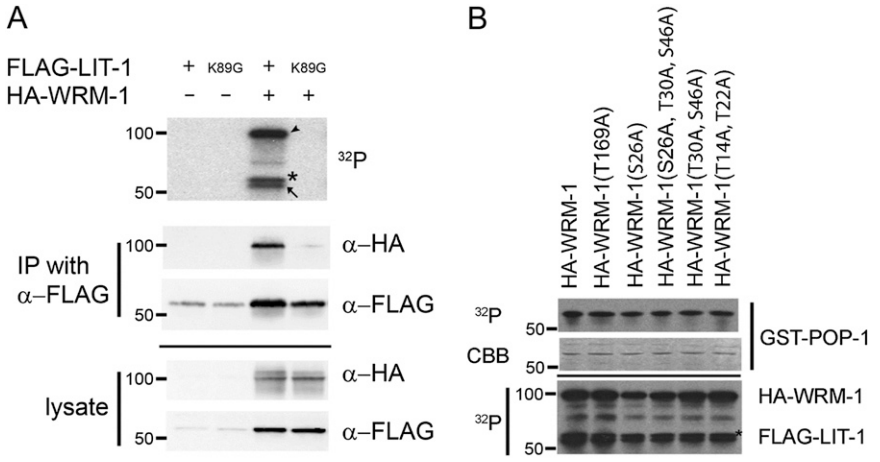

Fig. S4. In vitro LIT-1/WRM-1 kinase assays. (*A*) 293T cells were transfected with FLAG-LIT-1 WT (+) or catalytic mutant (K89G) expression plasmid with or without HA-WRM-1 expression plasmid (+ or −, respectively). FLAG-LIT-1/HA-WRM-1 complexes were immunoprecipitated with α-FLAG M2-agarose beads and assayed for in vitro kinase activity against GST-POP-1(1-188) proteins (*Top*; ^{32}P). The immunoprecipitates (*Middle*; IP with α-FLAG) and lysates (*Bottom*; lysate) were analyzed by Western blotting using α-HA or α-FLAG antibodies as indicated. As reported previously (1), FLAG-LIT-1 alone is an inactive kinase, whereas the FLAG-LIT-1/HA-WRM-1 complex is an active complex that specifically phosphorylates WRM-1 (indicated by the black arrowhead), LIT-1(indicated by the black arrow), and GST-POP-1 (indicated by the asterisk). The FLAG-LIT-1 catalytic mutant (K89G) does not form a stable complex with WRM-1. (*B*) 293T cells were transfected with FLAG-LIT-1 and HA-WRM-1 expression plasmids harboring various mutations affecting phosphorylation sites for GSK-3 (S26), CDK-1 (T30, S46), and potential MAPK sites (T14, T22, and T169). FLAG-LIT-1/HA-WRM-1 complexes were immunoprecipitated with α-FLAG M2-agarose beads and assayed for in vitro kinase activity against GST-POP-1 as in *A*. Phosphorylated GST-POP-1 protein was recovered from the kinase reactions using glutathione beads and analyzed by SDS/PAGE followed by CBB staining (*Middle*) and autoradiography (*Top*; ^{32}P). α-FLAG immunoprecipitates were analyzed for HA-WRM-1 and FLAG-LIT-1 complex formation and autophosphorylation (*Bottom*; ^{32}P). Asterisk indicates carry over GST-POP-1 protein. The formation of the FLAG-LIT-1/HA-WRM-1 complex and its kinase activity was not affected by any of the mutations in WRM-1 that were tested.

1. Rocheleau CE, et al. (1999) WRM-1 activates the LIT-1 protein kinase to transduce anterior/posterior polarity signals in C. elegans. *Cell* 97(6):717–726.

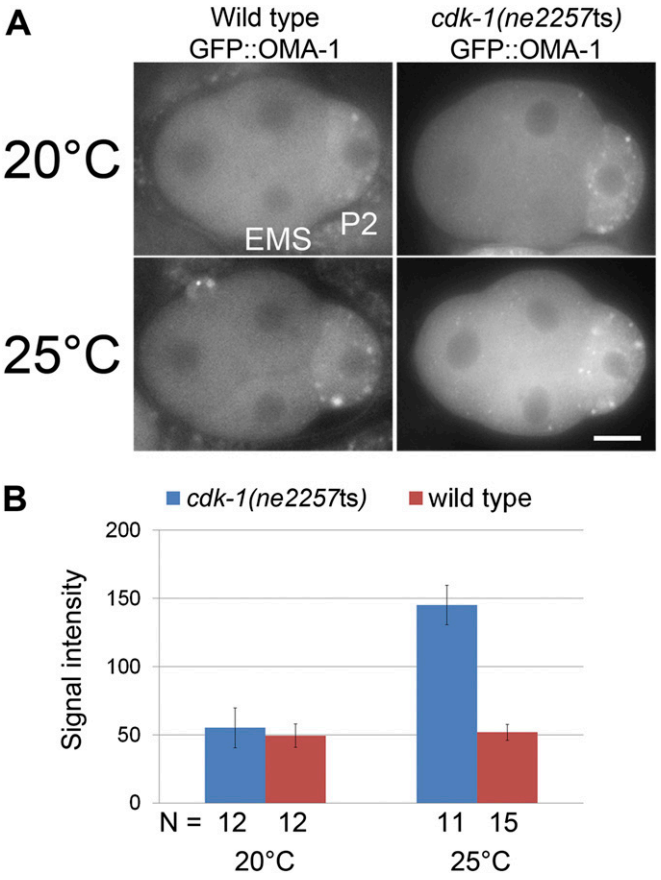

Fig. S5. OMA-1 protein level in four-cell *cdk-1*(*ne2257*ts) embryos. (*A*) Fluorescence micrographs of representative WT and *cdk-1*(*ne2257*ts) four-cell embryos expressing a *gfp::oma-1* transgene (gift from R. Lin) at the nonpermissive temperature (25 °C) or semipermissive temperature (20 °C). Anterior is to the left, and dorsal is up. (Scale bar: 10 μm.) (*B*) Quantification of OMA-1::GFP level was performed using ImageJ software. N, number of embryos scored. Error bars indicate SD.

Table S1. Cortical WRM-1 perturbs proper EMS division orientation

Embryo type	A (%)	B (%)	C (%)	Total *N*
src-1(RNAi)	73.8	16.5	9.7	115
mes-1(bn74)	100.0	0.0	0.0	9
mom-2(RNAi)	95.5	4.5	0.0	22
mom-2(ne834ts)	100.0	0.0	0.0	20
mom-5(RNAi)	94.6	2.7	2.7	37
mom-4(ne1539ts)	100.0	0.0	0.0	10
lit-1(RNAi)	100.0	0.0	0.0	18
lit-1(ne1991ts)	100.0	0.0	0.0	23
wrm-1(RNAi)	100.0	0.0	0.0	47
cdk-1(ne2257ts)	95.7	4.3	0.0	68
cdk-1(ne2257ts); src-1(RNAi)	15.6	20.0	64.4	90
cdk-1(ne2257ts); mom-2(RNAi)	100.0	0.0	0.0	22
cdk-1(ne2257ts); mom-5(RNAi)	100.0	0.0	0.0	15
cdk-1(ne2257ts); src-1(RNAi); lit-1(RNAi)	76.5	5.9	17.6	34
cdk-1(ne2257ts); src-1(RNAi); wrm-1(RNAi)	81.5	11.1	7.4	27
flag::wrm-1;wrm-1(tm514)	100.0	0.0	0.0	45
flag::wrm-1; wrm-1(tm514); mom-4(ne1539ts)	100.0	0.0	0.0	37
flag::wrm-1;wrm-1(tm514);src-1(RNAi)	76.0	22.0	2.0	76
flag::wrm-1; wrm-1(tm514);src-1(RNAi); mom-4(ne1539ts)	74.2	16.1	9.7	31
flag::wrm-1; wrm-1(tm514);src-1(RNAi); wrm-1(RNAi)	71.9	28.1	0.0	32
flag::wrm-1$_{T30AS46A}$; wrm-1(tm514)	100.0	0.0	0.0	46
flag::wrm-1$_{T30AS46A}$; wrm-1(tm514); mom-4(ne1539ts)	100.0	0.0	0.0	11
flag::wrm-1$_{T30AS46A}$; wrm-1(tm514); src-1(RNAi)	30.0	33.3	36.7	68
flag::wrm-1$_{T30AS46A}$; wrm-1(tm514); src-1(RNAi); mom-4(ne1539ts)	75.0	16.7	8.3	36
flag::wrm-1$_{T30AS46A}$; wrm-1(tm514); src-1(RNAi); wrm-1(RNAi)	74.3	22.9	2.8	35
*wrm-1**	100.0	0.0	0.0	10
wrm-1; src-1(RNAi)*	68.0	24.0	0.0	25
wrm-1; wrm-1(tm514)*	100.0	0.0	0.0	30
wrm-1; wrm-1(tm514); src-1(RNAi)*	58.9	38.5	2.6	39
wrm-1$_{T30AS46A}$*	100.0	0.0	0.0	10
wrm-1$_{T30AS46A}$; src-1(RNAi)*	23.0	38.5	38.5	26
wrm-1$_{T30AS46A}$; wrm-1(tm514)*	100.0	0.0	0.0	30
wrm-1$_{T30AS46A}$; wrm-1(tm514); src-1(RNAi)*	40.6	35.1	24.3	37
src-1(RNAi); mom-2(RNAi)	0.0	6.5	93.5	92
src-1(RNAi); mom-2(ne834ts)	15.2	15.2	69.6	33
src-1(RNAi); mom-2(RNAi); mom-4(ne1539ts)	68.2	13.6	18.2	22
src-1(RNAi); mom-2(RNAi); lit-1(ne1991ts)	28.1	46.9	25.0	32
src-1(RNAi); mom-2(ne834ts); wrm-1(RNAi)	64.3	14.3	21.4	28
mes-1(bn74); mom-2(ne834ts)	19.2	23.1	57.7	26
mes-1(bn74); mom-2(RNAi); mom-4(ne1539ts)	60.7	21.4	17.9	28
mes-1(bn74); mom-2(RNAi); lit-1(ne1991ts)	65.6	18.8	15.6	32
mes-1(bn74); mom-2(ne834ts); wrm-1(RNAi)	76.9	9.6	13.5	52

Orientation of EMS mitotic spindle was measured as explained in Fig. 2 and *Materials and Methods*. This table compiles data from Figs. 2 and 4, part of Fig. 5, and additional genetic combinations and controls. Details on the scoring method are in *Materials and Methods*. Phenotypes of some relevant single and double mutants were described in ref. 1.

*Strains expressing *wrm-1* transgenes without an epitope tag (*wrm-1** and *wrm-1*$_{T30AS46A}$*).

1. Bei Y, et al. (2002) SRC-1 and Wnt signaling act together to specify endoderm and to control cleavage orientation in early C. elegans embryos. *Dev Cell* 3(1):113–125.

Table S2. Statistical analysis of the EMS mitotic spindle orientations (multiple-comparisons ANOVA with Bonferroni posthoc analysis)

Category of EMS cell division	RNAi	Population 1	Population 2	*P* value
C	*src-1*	WT	*flag::wrm-1; wrm-1(tm514)*	0.597
C	*src-1*	WT	*flag::wrm-1$_{T30AS46A}$; wrm-1(tm514)*	0.003
C	*src-1*	*flag::wrm-1; wrm-1(tm514)*	*flag::wrm-1$_{T30AS46A}$; wrm-1(tm514)*	<0.001
C	*wrm-1*	WT	*flag::wrm-1; wrm-1(tm514)*	1.000
C	*wrm-1*	WT	*flag::wrm-1$_{T30AS46A}$; wrm-1(tm514)*	1.000
C	*wrm-1*	*flag::wrm-1; wrm-1(tm514)*	*flag::wrm-1$_{T30AS46A}$; wrm-1(tm514)*	1.000
C	*src-1 wrm-1*	WT	*flag::wrm-1; wrm-1(tm514)*	0.001
C	*src-1 wrm-1*	WT	*flag::wrm-1$_{T30AS46A}$; wrm-1(tm514)*	0.045
C	*src-1 wrm-1*	*flag::wrm-1; wrm-1(tm514)*	*flag::wrm-1$_{T30AS46A}$; wrm-1(tm514)*	0.011
B	*src-1*	WT	*flag::wrm-1; wrm-1(tm514)*	0.910
B	*src-1*	WT	*flag::wrm-1$_{T30AS46A}$; wrm-1(tm514)*	0.117
B	*src-1*	*flag::wrm-1; wrm-1(tm514)*	*flag::wrm-1$_{T30AS46A}$; wrm-1(tm514)*	0.271
B	*wrm-1*	WT	*flag::wrm-1; wrm-1(tm514)*	1.000
B	*wrm-1*	WT	*flag::wrm-1$_{T30AS46A}$; wrm-1(tm514)*	1.000
B	*wrm-1*	*flag::wrm-1; wrm-1(tm514)*	*flag::wrm-1$_{T30AS46A}$; wrm-1(tm514)*	1.000
B	*src-1 wrm-1*	WT	*flag::wrm-1; wrm-1(tm514)*	0.185
B	*src-1 wrm-1*	WT	*flag::wrm-1$_{T30AS46A}$; wrm-1(tm514)*	0.164
B	*src-1 wrm-1*	*flag::wrm-1; wrm-1(tm514)*	*flag::wrm-1$_{T30AS46A}$; wrm-1(tm514)*	0.466

P values are reported for multiple comparisons of categories B and C between the strains specified. We used Bonferroni posthoc testing to correct for multiple comparisons.